

# Friction Stir Processing of 304L Stainless Steel for Crack Repair

M.P. Miles, C. Gunter, F. Liu and T.W. Nelson

**Abstract** Friction stir processing (FSP) was investigated as a method for repairing cracks in 304L stainless steel. Healing feasibility was demonstrated by processing a tapered crack and a series of randomly sequenced cracks with different widths. It was possible to heal a crack that begins narrow and then progressively widens, but processing a crack that starts too wide created voids that could not be closed up. Tension and hardness testing of 304L plates processed under different conditions were performed in order to assess the effect of processing on weld and heat affected zone properties. Corrosion testing was also carried out, in order to evaluate the effect of FSP on potential sensitization of the stir zone. After 1000 h of testing in saline solution at room temperature it was found that no corrosion products formed on the base material controls or on any of the friction stir processed specimens.

**Keywords** 304L stainless steel • Friction stir processing • Crack healing

## Introduction

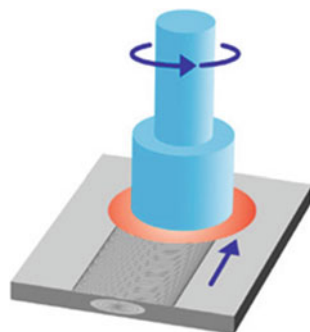
The nuclear industry is facing challenges in repair or replacement of stainless steel reactor components, which have been exposed to neutron irradiation. Irradiated stainless steel contains helium, which forms primarily by  $n/\alpha$  reactions with alloying elements nickel and boron [1–6]. Helium gas is insoluble in metals, so it precipitates and forms bubbles (at the nanoscale), nucleating at dislocations, point defects, and grain boundaries [4]. When conventional fusion welding is used for weld repair, the high temperatures and thermal stresses inherent in the process

---

M.P. Miles (✉) • C. Gunter  
Manufacturing Engineering Technology, Provo, USA  
e-mail: mmiles@byu.edu

F. Liu • T.W. Nelson  
Mechanical Engineering, Provo, USA

**Fig. 1** FSP could be used to repair a crack by processing an existing arc weld



enhance the growth of helium bubbles, causing intergranular cracking in the heat-affected zone (HAZ) [6–8].

Repair of nuclear components encompasses both the replacement of a failed component, in which case a new component must be joined to existing structures, and the in situ repair of arc welds that have developed stress corrosion cracks in service [2, 9, 10]. In both cases the issue of helium embrittlement, accelerated by the temperatures and stresses of fusion welding, presents a serious difficulty that must be overcome. While low heat input laser welding can be a partial solution to the problem [7], reactors with 30–40 years of service may have irradiated components which cannot be repaired by any of the conventional methods [11]. It is anticipated that many nuclear reactors will function for up to 80 years [12], so the reparability of irradiated stainless steel is of great importance to this industry.

Friction stir processing (FSP) is similar to friction stir welding (FSW), except that its purpose is not to join parts together, but to modify material microstructures and properties. The repair of a stress corrosion crack in an existing weld could be done by passing a tool along an existing weld or HAZ and “healing” the crack. The process of FSP is shown in Fig. 1.

Much of the prior work done in FSW can be applied to FSP. Both FSW and FSP have been studied extensively for their ability to create favorable properties in metal alloys [13–19], most of which have been aluminum alloys. While we have not found research literature on the use of FSP to “heal”, or repair, stress corrosion cracks in existing welds, one study by Sterling demonstrated that FSP can be used to process over existing arc welds in austenitic stainless steel, to enhance the mechanical properties of the weld [20]. For stress corrosion crack repair of irradiated stainless steel, lower peak temperatures would favor the use of FSP over fusion welding processes like GTAW, because the helium bubbles present in the material would have a lower driving force to diffuse to grain boundaries in the HAZ. But if FSP is a potential solution for weld repair of irradiated stainless steel, there remains the potential challenge of sigma phase and chromium carbide formation, which have been reported in friction stir welded 304L stainless steel along the advancing side of the stir zone [21]. Although others have reported preferential etching along this same region of the stir zone, they also report large variability, depending on the welding conditions [20, 22]. Sigma and chromium carbide phases

are well known to reduce the corrosion resistance of austenitic stainless steel [21–23], and need to be suppressed if FSP is to be employed for weld repair.

## Experimental Procedures

FSP experiments were performed on 12 mm thick 304L stainless steel using a tool speed of 250 rpm and a feed rate of 100 mm/min. The tool, provided by Megastir Technologies, was composed of 70% PCBN and 30% W-Re, with a pin length of 8 mm and a convex 25 mm diameter shoulder, as shown in Fig. 2. The pin was threaded and the shoulder had scrolls, in order to promote the stirring of material.

The microstructure in the initial plate exhibited an average grain size of about 40  $\mu\text{m}$ , but some grains were as small as 5  $\mu\text{m}$ , as measured by electron backscatter diffraction (EBSD), shown in Fig. 3.

**Fig. 2** Friction stir processing tool (70% PCBN/30% W-Re), with an 8 mm long conical pin and 25 mm diameter convex shoulder



**Fig. 3** 304L stainless steel microstructure for as-received plate

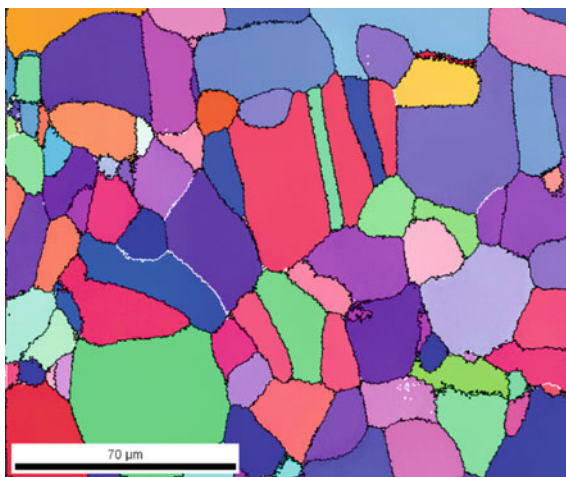


**Table 1** Composition of 304L stainless steel (wt%)

C	Mn	P	S	Si	Cr	Ni	N	Fe
0.08	2.00	0.045	0.030	0.75	18–20	8–12	0.10	Balance

The composition of the plates that were processed is shown in Table 1.

Experiments were done in order to assess both the crack healing capability of FSP and to measure the mechanical properties of specimens that had been processed using a variety of different tool feeds and speeds.

## Results and Discussion

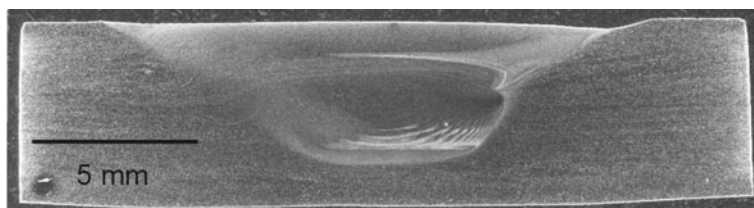
Two different crack healing experiments were carried out. The first one employed a plate with a variety of different machined cracks, randomly place along a straight line in a 304L plate. Each crack was 30 mm long and went through the full thickness of the plate. The crack widths, in sequence, were: 3 mm, 0.5 mm, 2.0 mm, 2.5 mm, 1.5 mm, 1.0 mm, 0.33 mm. With random ordering, the 3 mm crack was the first one in the sequence, which proved to be too wide to heal. Therefore, the first experiment didn't provide much information about crack healing feasibility using FSP. A second experiment was performed on a tapered crack, where the tool started processing at the narrow end and finished processing at the wide end (0 mm at the beginning and 2 mm at the end). The simulated crack was cut by wire EDM and was 400 mm long.

Figure 4 shows a sequence of cross sections spaced along the length of the crack. The oxide layer at the joint interface is clearly seen in each cross section. The stir zone shows adequate healing of the crack throughout the sequence; however, as the crack approaches a width of 2 mm, there is less material to be consolidated and a depression develops on the top of the plate, on the advancing side (right side) of the stir zone.

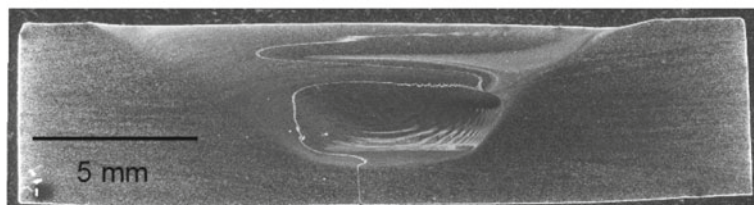
From these results it appears that cracks in 304L can be healed by FSP, up to about 2 mm in width, using the tool design shown in Fig. 2 and parameters of 250 rpm—100 mm/min. Further work is needed to characterize properties of specimens where crack healing has taken place by FSP.

In addition to crack healing, some bead-on-plate FSP experiments were performed at different feeds and speeds. Mechanical properties and hardness of the stir zone were assessed for each set of parameters, and grain sizes were measured on the advancing side (AS), center (C), and retreating side (RS) of the stir zone.

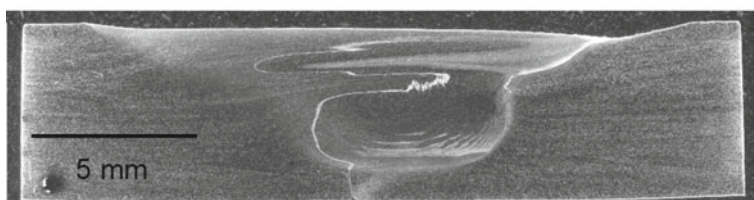
Cross sections of the plates processed at different feeds and speeds are shown in Fig. 5. Most of the parameters resulted in a consolidated stir zone except for the plates processed at 125 rpm—150 mm/min (easily visible) and 175 rpm—150 mm/min (much smaller voids), both of which had voids in the lower portion of the advancing side nugget (Fig. 5b).



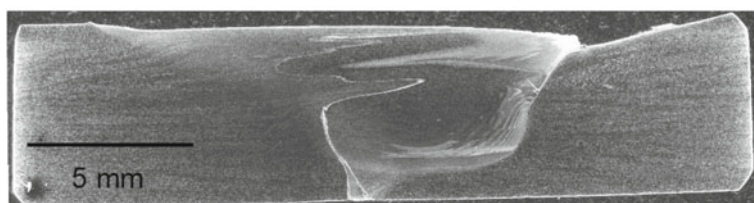
(a)



(b)



(c)



(d)

**Fig. 4** Cross sections of tapered crack healing experiment. **a** base material just before the crack, **b** 45 mm from beginning of tapered crack, **c** 205 mm from beginning of crack, **d** 385 mm from beginning of crack

Transverse tensile testing (weld transverse to major strain axis) was carried out, using three specimens for each set of parameters. A summary of the testing is shown in Table 2, along with the power measured at the spindle of the machine during the FSP experiments.

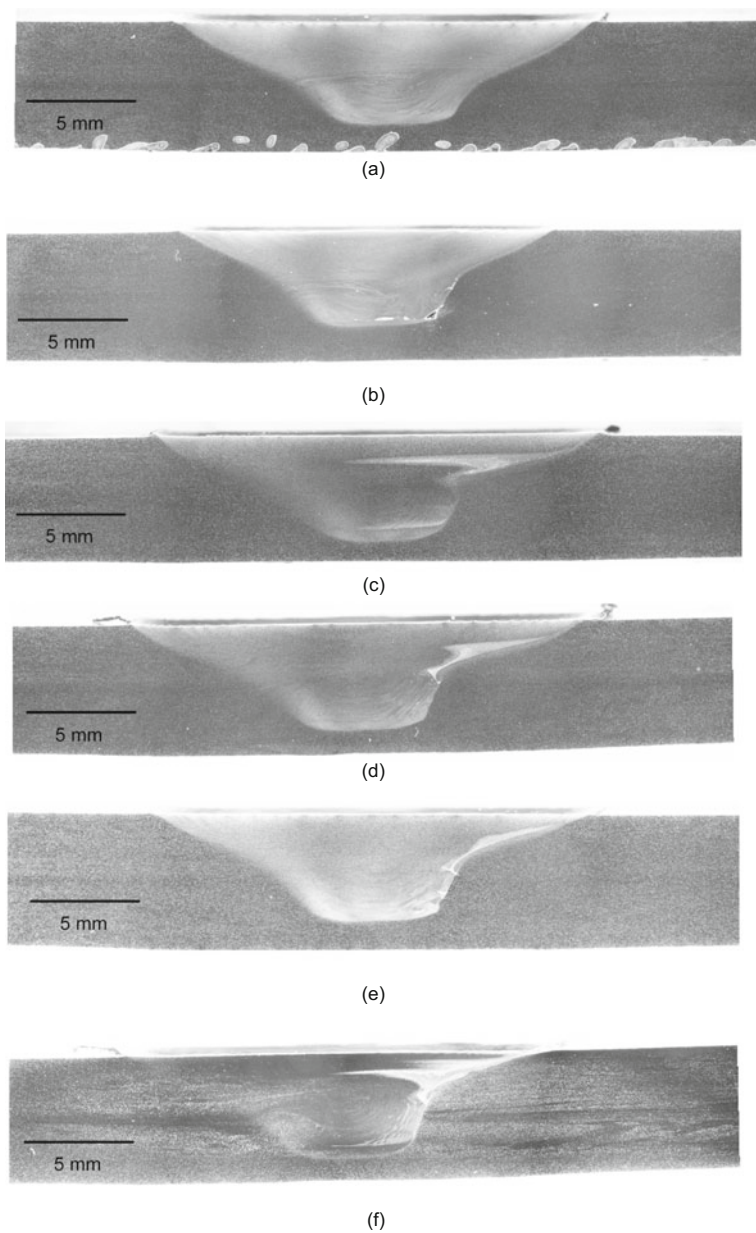


**Fig. 5** Cross sections of bead-on-plate stir zones for different parameters. **a** 80 rpm—50 mm/min, **b** 125 rpm—150 mm/min, **c** 150 rpm—50 mm/min, **d** 150 rpm—100 mm/min, **e** 175 rpm—150 mm/min, **f** 250 rpm—100 mm/min

**Table 2** Mechanical properties for transverse tensile specimens (average of 3 specimens)

FSP parameters	FSP power (kW)	% Total elongation	Ultimate tensile strength (MPa)
Base metal	–	76	622
80 rpm—50 mm/min	3.3	49	696
125 rpm—150 mm/min	4.8	39	683
150 rpm—50 mm/min	4.9	59	684
150 rpm—100 mm/min	6.3	62	429
175 rpm—150 mm/min	4.8	22	675
250 rpm—100 mm/min	6.3	27	605

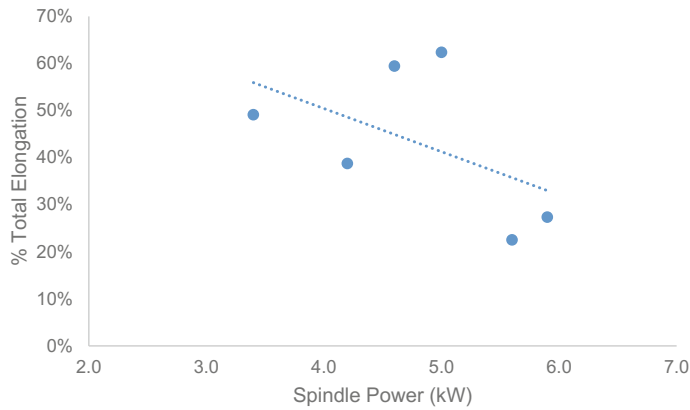


**Fig. 6** Total elongation in transverse tensile test as a function of FSP power

From an elongation viewpoint, the worst performance corresponded to the parameters that generated the greatest power at the welding spindle. Although temperatures in the stir zone cannot be measured directly, power correlates positively with welding temperature. Tensile elongation correlated negatively with welding power ( $R^2 = 0.44$ ) in this case, as seen in Fig. 6. All welded specimens had elongations that were less than base material, while four of the specimens had a UTS higher than the base material.

Grain sizes in the stir zone were measured by EBSD, while microhardness measurements were made in the stir zone and in the base material. The data from these measurements are shown in Table 3, along with spindle power for each case.

For a given set of parameters grain sizes varied but were essentially similar on the retreating side, center, and advancing side of the stir zone, given the large standard deviations in the measurements. All grain sizes in the stir zone represent grain refinement compared to the base material average grain size of about 40  $\mu\text{m}$ .



**Table 3** Grain sizes in stir zone and microhardness ranges across stir zone, heat affected zone, and base material

			Grain size			$\mu$ -Hardness (HV)	
Feed rate (mm/min)	RPM	Spindle power (KW)	RS	C	AS	Min	Max
50	80	3.3	$2.72 \pm 1.39$	$2.91 \pm 1.54$	$2.77 \pm 1.42$	186	318
50	150	4.8	$7.97 \pm 4.16$	$9.03 \pm 4.87$	$9.32 \pm 4.94$	184	246
100	150	4.9	$5.63 \pm 2.86$	$6.47 \pm 3.41$	$5.51 \pm 2.78$	188	272
100	250	6.3	$9.25 \pm 5.5$	$9.70 \pm 5.27$	$11.35 \pm 6.17$	184	265
150	125	4.8	$2.04 \pm 0.94$	$2.63 \pm 1.46$	$2.43 \pm 1.18$	180	340
150	175	6.3	$4.73 \pm 2.37$	$5.61 \pm 3.09$	$5.63 \pm 2.86$	182	302

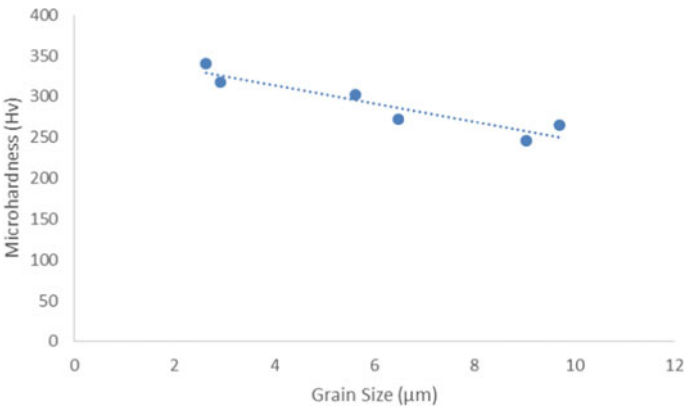


**Fig. 7** Stir zone microhardness as a function of grain size

However, across the different parameter sets grain sizes were larger for cases of greater spindle power, although the relationship is not linear. Maximum hardness values did correlate somewhat negatively with spindle power ( $R^2 = 0.10$ ). But as expected from the Hall-Petch relationship, finer grain size was strongly correlated with greater microhardness, as seen in Fig. 7.

Conclusions

Feasibility of crack repair by FSP was demonstrated in 12 mm thick 304L stainless steel plate. The repair of a tapered, straight crack, machined through the plate thickness by wire EDM, was evaluated visually by examining cross sections along the length of the stir zone. In this case, it appears that 2 mm crack width is the



practical limit for repair, since the top of the stir zone exhibited a depression on the advanced side, owing to the lack of material represented by the crack. Bead on plate FSP experiments on 12 mm 304L plate showed a negative relationship between spindle power and total elongation in transverse tensile specimens, while the UTS of the same specimens were greater than that of the base material in 4 out of 6 cases. Inhomogeneity of hardness in the friction stir processed specimens is the reason for lower total elongations compared to the base material. Finer grain size in the stir zone was strongly correlated with greater levels of hardness, as would be expected from the Hall-Petch relationship.

**Acknowledgements** This work was supported by National Science Foundation grant CMMI-1405508.

## References

1. Asano K et al (1999) Weldability of neutron irradiated austenitic stainless steels. *J Nucl Mater* 264(1–2):1–9
2. Kanne WR et al (1999) Weld repair of irradiated materials. *Mater Charact* 43(2–3):203–214
3. Tsuchiya K, Kawamura H, Kalinin G (2000) Re-weldability tests of irradiated austenitic stainless steel by a TIG welding method. *J Nucl Mater* 283:1210–1214
4. Li S et al (2011) The effect of helium on welding irradiated materials. *Weld J* 90(1):19S–26S
5. Tosten MH et al (2007) Repair techniques for fusion reactor applications. *Weld J* 86(8):245S–252S
6. Feng Z, Wilkowski G (2002) Repair welding of irradiated materials: modeling of helium bubble distributions for determining crack-free welding procedures. Medium: X; Size: 8 pp
7. Yurioka N, Horii Y (2006) Recent developments in repair welding technologies in Japan. *Sci Technol Weld Joining* 11(3):255–264
8. Kanne WR et al (1995) Welding irradiated stainless-steel. *J Nucl Mater* 225:69–75
9. Wang CA et al (1996) The effect of an applied stress on the welding of irradiated steels. *J Nucl Mater* 239(1–3):85–89
10. Wang CA et al (1996) Welding of irradiated stainless steel. *J Nucl Mater* 233:213–217
11. Willis, E., *Electrical Power Research Institute (EPRI)*. 2013
12. Li S et al (2011) The effect of helium on welding of irradiated materials. *Weld J* 90:7
13. Yang Q, Xiao BL, Ma ZY (2012) Influence of process parameters on microstructure and mechanical properties of friction-stir-processed Mg-Gd-Y-Zr casting. *Metall Mater Trans a-Phys Metall Mater Sci* 43A(6):2094–2109
14. Tsai FY, Kao PW (2012) Improvement of mechanical properties of a cast Al-Si base alloy by friction stir processing. *Mater Lett* 80:40–42
15. Sun N, Apelian D (2011) Friction stir processing of aluminum cast alloys for high performance applications. *JOM* 63(11):44–50
16. Feng XL, Liu HJ, Babu SS (2011) Effect of grain size refinement and precipitation reactions on strengthening in friction stir processed Al-Cu alloys. *Scripta Mater* 65(12):1057–1060
17. Liu FC, Ma ZY (2010) Contribution of grain boundary sliding in low-temperature superplasticity of ultrafine-grained aluminum alloys. *Scripta Mater* 62(3):125–128
18. Liechty BC, Webb BW (2008) Modeling the frictional boundary condition in friction stir welding. *Int J Mach Tools Manuf* 48(12–13):1474–1485
19. Mishra RS, Ma ZY (2005) Friction stir welding and processing. *Mater Sci Eng: R: Rep* 50(1–2):1–78

20. Sterling CJ et al (2004) Effects of friction stir processing on the microstructure and mechanical properties of fusion Welded 304L Stainless Steel, in Research Report. Office of Naval Research. p 7
21. Park SHC et al (2003) Rapid formation of the sigma phase in 304 stainless steel during friction stir welding. *Scripta Mater* 49(12):1175–1180
22. Sorensen CD, Nelson TW (2005) Sigma phase formation in friction stirring of iron-nickel-chromium alloys. In: proceedings of the 7th international conference on trends in welding research. Pine Mountain, GA: ASM
23. Park SHC et al (2004) Corrosion resistance of friction stir welded 304 stainless steel. *Scripta Mater* 51(2):101–105

Friction Stir Welding and Processing IX

Hovanski, Y.; Mishra, R.; Sato, Y.; Upadhyay, P.; Yan, D.  
(Eds.)

2017, XIV, 324 p. 245 illus., Hardcover

ISBN: 978-3-319-52382-8